Mater. Res. Soc. Symp. Proc. Vol. 1536 © 2013 Materials Research Society
DOI: 10.1557/opl.2013.910

Stress Analysis of Free-Standing Silicon Oxide Films Using Optical Interference

Imen Rezadad*, Javaneh Boroumand, Evan Smith, Pedro Figueiredo, Robert E. Peale
Department of Physics, University of Central Florida, Orlando, FL, USA 32816

ABSTRACT

We report a method for stress measurement and analysis in silicon oxide thin films using optical interference. Effects of design and fabrication on stress have been studied by fabricating submicron-thick slabs of oxide anchored at one end and extending over a reflective surface. Optical interference occurs between reflections from the surface and the oxide slab, giving rise to light and dark fringes that may be imaged with a microscope. Analysis of the interference pattern at different wavelengths gives the radius of curvature and means of stress mapping. The accuracy exceeds non-interferometric profilometry using optical or confocal microscopes, and it can be more quantitative than scanning electron microscopy. This nondestructive profilometry method can aid the stress optimization of silicon oxide or other transparent thin films to achieve specific mechanical characteristics in MEMS devices.

INTRODUCTION

We report an optical interference method to measure stress in a silicon dioxide thin film. This method is based on observation of Fizeau fringes [1] that are caused by interference of reflected light between a curved semi-reflective silicon dioxide thin film and a flat reflective surface beneath it. Fizeau interferometry is widely used to compare the shape of an optical surface on a mirror or lens to a reference surface of known shape [2]. The two surfaces are separated by a narrow gap, and interference fringes in reflected monochromatic light indicate spatial variations of the gap. Among other applications are thickness measurement of thin films, strain measurement of fiber optics, residual wedge measurement for optical flats and characterization of organic light emitting devices [3-6].

Stress is important to free-standing thin films in MEMS due to the deformations it induces, intended or otherwise. Intrinsic stresses, which depend on deposition conditions, are difficult to predict. Usual methods to measure stress in a thin film require measurement of the radius of curvature of a large substrate (e.g. a wafer) on which the film has been deposited and to which it is firmly attached [7]. This can be either done by a contact profiler, which can damage soft and suspended features, or by noncontact profilers, which can be expensive and slow.

We are interested in controlling the stress and deformation in free standing MEMS cantilevers, which consist of a 500 nm thick oxide topped with 30 nm of Cr/Au above a gold surface plate (Figure 1). Observed Fizeau fringes allow observation of height and curvature, as shown in Figure 1 (right). Cantilever motion and curling appear as a change in the fringe pattern. These cantilevers tend to curl upward after the metal deposition and release due to the different thermal expansion coefficients of metal and oxide. The curvature depends on the oxide deposition recipe, where different methods give different intrinsic stress, and on the temperature of the sample during deposition.

The 500 nm low stress silicon dioxide was deposited by Trion Orion II PECVD system using TEOS gas on top of a polyimide sacrificial layer. The cantilever legs are attached to the substrate via small square anchors. Photolithography, e-beam evaporation of 5 nm Cr and 25 nm

Au, and lift-off creates a dry etch mask for both oxide (CF_4 etch) and polyimide layers (O_2 etch). After release we obtain the structure imaged by scanning electron microscopy (SEM) in Figure 1 (left). Figure 1 (right) shows an optical microscope image of a different cantilever in monochromatic light showing Fizeau fringes in the form of rings. To characterize the results of experiments, we developed the optical interferometric method described in this paper.

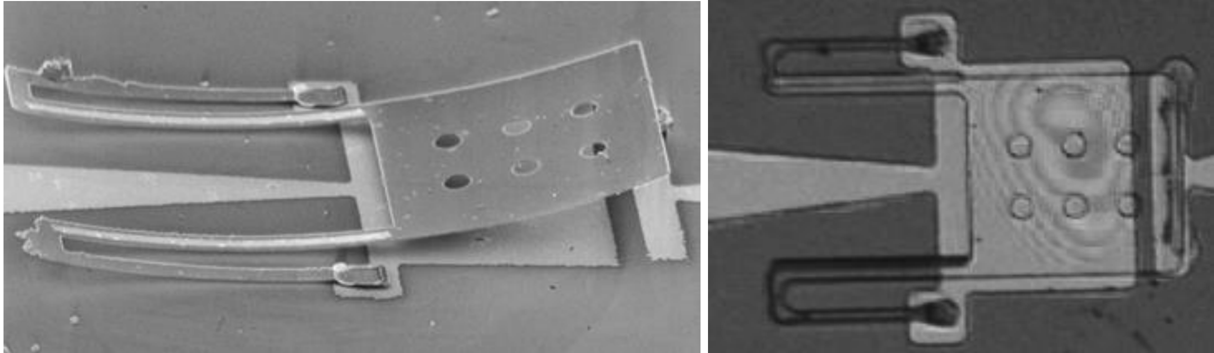

Figure 1 (left) - SEM image of 500 nm thick SiO_2 cantilever with semitransparent Au surface coating suspended over a Au surface plate. The cantilever is curled up due to intrinsic oxide stress and to differential thermal expansion, since the sample temperature exceeded ambient during the Au deposition. (Right) Optical microscope image in monochromatic light, showing Fizeau fringes.

EXPERIMENTAL DETAILS

Simplified cantilevers with a range of widths and lengths were fabricated. Figure 2 (left) presents a schematic of the processing steps. We spin-coated a Si wafer with 1.2 um ProLift-100 as polyimide sacrificial layer, and then 600 nm PMMA (495 A) was spin-coated on top. The desired pattern was exposed by electron-beam to define 10 micron square anchors. The PMMA was developed by MIBK:IPA 1:3 solution and ProLift was etched 15 s with TMAH based developer MF319 following by 75 sec dry etch in plasma enhanced etcher with O_2 gas. Longer wet etch undercuts the ProLift. PMMA was stripped in acetone, and 500 nm TEOS-based silicon oxide was deposited on the ProLift using the Trion PECVD system. The recipe was optimized to achieve high step coverage to strengthen the anchor neck points. The cantilever etch mask was produced by another PMMA spin, e-beam exposure, and MIBK:IPA development, followed by 42 nm sputtered Au and lift off. The Au serves as the reactive ion etch (RIE) mask for etching the oxide in CF_4 gas. The last steps to release the cantilevers are 2 min anisotropic etch of Prolift in RIE system using O_2 gas mixed with 6% CF_4 (300 W, 100 mTorr) and 10 min isotropic etch (300 W, 300 mTorr) while the sample is tilted 45 deg [8]. Figure 2 (right) presents an optical microscope image of the resulting cantilever array.

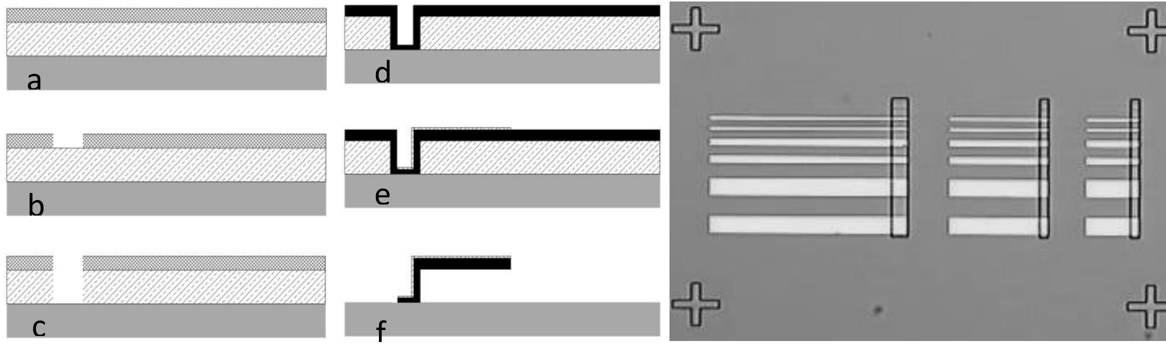

Figure 2 (left) Fabrication steps of cantilevers: a. Spin Prolift 100-2 as sacrificial layer, then PMMA; b. Pattern PMMA using e-beam writer and development in MIBK:IPA solution; c. Transfer pattern to sacrificial layer using combination of wet and dry etch; d. PECVD SiO_2; e. Patterned Au lift-off to achieve oxide etch mask; f. Etch oxide in RIE, then release in O_2 plasma RIE. (right) Optical microscope image of cantilever arms with length 55, 120, and 250 micron and with width 1, 5, 10, and 25 micron. The narrowest arms are invisible in this image. All arms are anchored at one end. The image was collected before etching the oxide and release from the sacrificial layer.

Fizeau fringes were recorded with a microscope equipped with a digital CCD camera. Images were analyzed in Labview to obtain line intensity profiles. To enhance fringe visibility and allow quantitative analysis, either a monochromatic laser or narrow band-pass filtered white light were used for illumination (Figure 3).

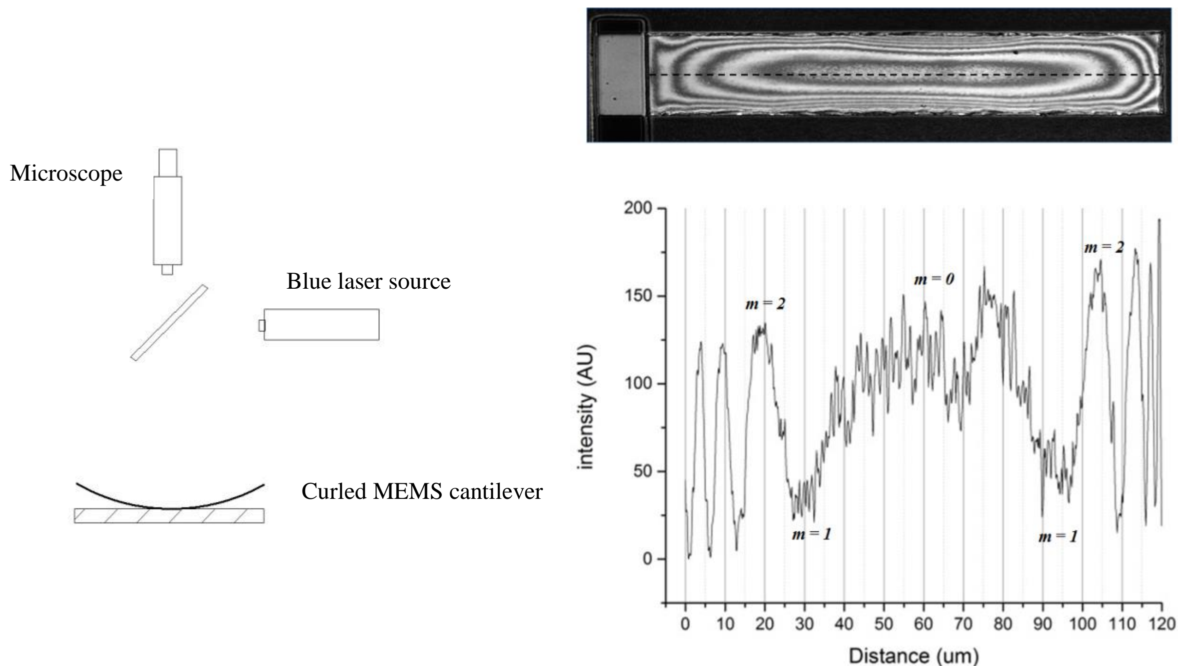

Figure 3 (left) – Schematic of set-up for observing Fizeau fringes. (right) Microscope image of cantilever with results of indicated intensity line-scan.

THEORETICAL CONSIDERATIONS

The optical boundaries that reflect light in the Figure 2 structures are the top Au surface, the Au/SiO_2 boundary, the SiO_2-air boundary underneath the cantilever, and the Si substrate surface. Interference between reflections from the top three parallel surfaces gives no fringes. Fringes due to interference come only between reflected light from Si substrate surface and light reflected from the cantilever as a whole. The latter reflection has some amplitude and phase whose exact values are unimportant. Amplitude affects fringe visibility while a shift in phase is equivalent to a uniform height offset between cantilever and substrate. We are only interested in height differences from different parts of the structure, which for adjacent light and dark fringes is just half a wavelength $\lambda/2$.

The profile of small deformations may be considered as the arc of a circle of radius R, as shown in the Figure 4 schematic. Stoney's formula [9] relates radius of curvature in a double layer structure to the stress in the film as

$$\sigma^{(f)} = \frac{E_{SiO2}}{6(1-\nu_{SiO2})} \times \frac{h_{SiO2}^2}{R h_{Au}} \tag{1}$$

where E and ν are Young's modulus and Poisson's ratio respectively and h is the layer thickness. This formula is valid when $h_{Au} \ll h_{SiO2} \ll R$. The height differences d_m above the minimum at the position of the mth ring is $m\lambda/2$, where m is an integer that is incremented with each new light or dark ring counting from the central spot ($m = 0$). See Figure 3 for an example of how the rings are numbered. Across a cantilever d_m generally amounts to only several half wavelengths, i.e. no more than a few microns, while ring radii r_m are on the scale of 10s of microns, according to Figure 3. In this limit of $d_m \ll r_m$, $R \approx \frac{r^2}{2d}$ according to Figure 4 so that Eq. 1 becomes

$$\sigma^{(f)}(r) = \frac{E_{SiO2}}{6(1-\nu_{SiO2})} \times \frac{h_{SiO2}^2}{h_{Au}} \times \frac{m\lambda}{r_m{}^2} \quad . \tag{2}$$

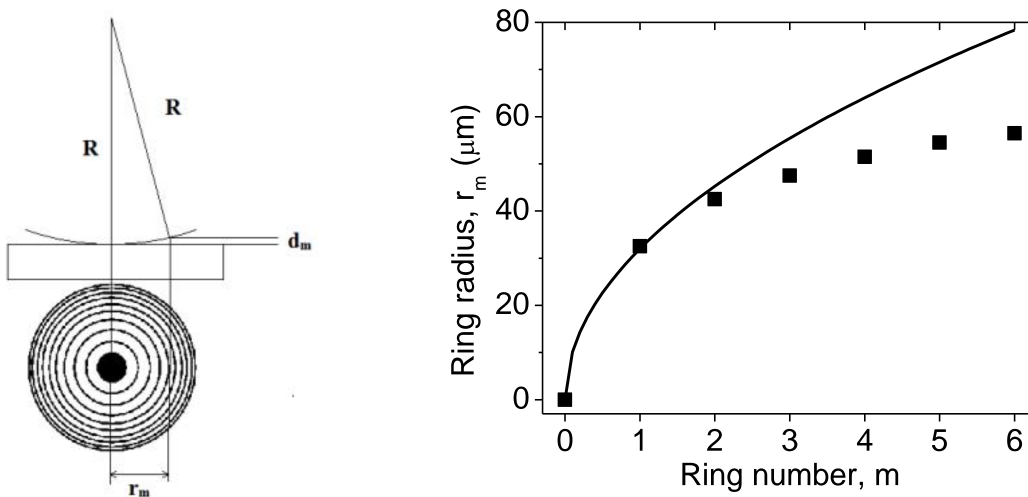

Figure 4 – (left) Schematic with air gap d_m, ring radius r_m, and radius of curvature R. (right) ring radius r_m vs. ring number m for Figure 3 profile (symbols) and function $\mathbf{32\sqrt{m}}$ (line).

RESULTS AND DISCUSSION

The assumption that the deformation along a particular direction is the arc of a circle means the stress has the same value at every point along that direction. In other words, uniform σ has no m dependence, which requires r_m to increase as the square root of m according to Eq. 2. For the example of Figure 4 (right), the experimental r_m values rise more slowly than $\sqrt{m}$, which implies that stress is higher near the edges. In other words, closer ring spacing means more curling, which implies higher stress. For other directions the stress might be lower at the edges. That stress is not uniform is supported by Figure 5, where the Fizeau rings even lack the same symmetry as the cantilever, one corner being strongly curled.

Figure 5a presents an SEM image of one of the fabricated arms. Curling of the lower right corner is obvious, but it is clearly impossible from this image to quantify the deformation. Figure 5b presents the Fizeau fringes for the same arm at 408 nm wavelength. To obtain a map of stress over the surface, a radial mesh was drawn from the center dark fringe to the boundaries and the position of each dark and bright fringe was determined along each line. Figure 5c is the resulting contour plot of the d_m in units of μm. Figure 5d gives the stress distribution over the surface calculated according to Eq. 2, where the darkest shade indicates 111 MPa and the lightest 753 MPa The stress is highest along the short direction and at the curled corner and lowest in the long direction. During release a tilted sample helps RIE removal of hard baked Prolift. This may explain the asymmetry of the deformation [10].

In summary, we have presented a method of measuring topography, stress (and motion) of free standing transparent films with high spatial resolution and without special instrumentation.

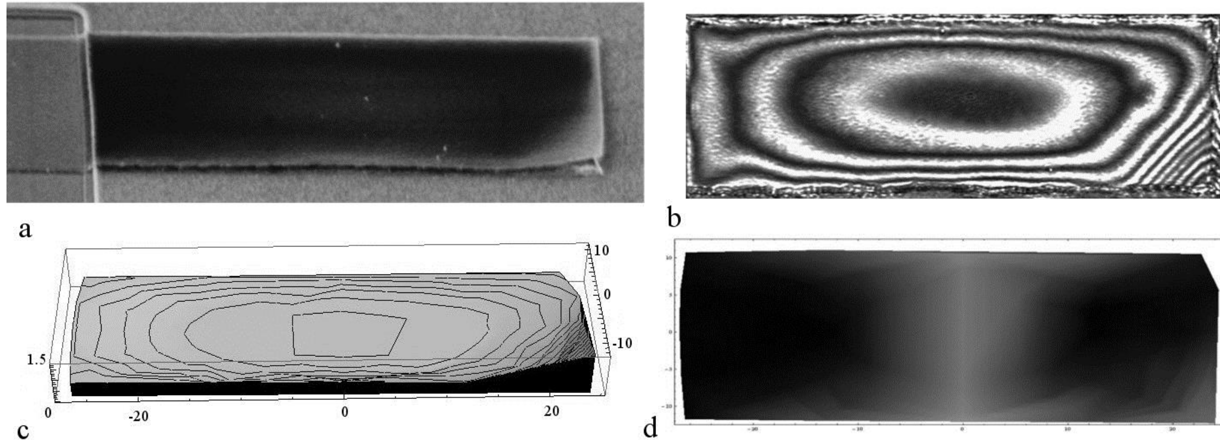

Figure 5 – a. SEM image of an arm after release b. Image taken with 408 nm wavelength source revealing fringe pattern. c. Contour plot. d. Calculated stress map on the surface of cantilever, bright areas shows higher stress values.

ACKNOWLEDGMENTS

This work was supported in part by a contract EMX International LLC, and by a grant from the Florida High Technology Corridor (I-4) program. Travel to attend this meeting was supported by UCF Graduate Studies and the UCF Student Government Association.

REFERENCES

1. A. Reserbat-Plantey, L. Marty, O. Arcizet, N. Bendiab, V. Bouchiat, Nature Nanotechnology 7, 151 (2012).
2. NASA preferred reliability practices. GUIDELINE NO. GT-TE-2404, NASA Technical Memorandum 4322A, NASA Reliability Preferred Practices for Design and Test, (NASA Office of Safety and Mission Assurance, Washington, 1999).
3. J. G. Gottling and W. S. Nicol, JOSA 56, 1227 (1966).
4. E. Li, G. Peng, X. Ding, Appl. Phys. Lett. 92, 101117 (2008).
5. S. Chatterjee, Opt. Eng. 42, 3235 (2003).
6. C. Tsai, K. Tien, M. Chen, K. Chang, M. Lin, H. Cheng, Y. Lin, H. Chang, H. Lin, C. Lin, C. Wu, Organic Electronics 11, 439 (2010).
7. T. M. Adams and R. A. Layton, *Introductory MEMS: Fabrication and Applications* (Springer, Berlin, 2010).
8. J. Boroumand Azad, I. Rezadad, J. Nath, E. Smith, R. E. Peale, Proc. SPIE 8682-80 (2013).
9. G. G. Stoney, Proc. R. Soc. London, Ser. A 82,172 (1909).
10. A. A. Volinsky, G. Kravchenko, P. Waters, J. D. Reddy, C. Locke, C. Frewin, S. E. Saddow in *Residual Stress in CVD-grown 3C-SiC Films on Si Substrates,* edited by M. Law, B. J. Pawlak, M. L. Pelaz, K. Suguro (Mater. Res. Soc. Symp. Proc. 1069, 1065-D03-05, 2008)